PHYSICAL REVIEW B **94**, 241111(R) (2016)

Quantum critical point of Dirac fermion mass generation without spontaneous symmetry breaking

Yuan-Yao He,[1] Han-Qing Wu,[1] Yi-Zhuang You,[2] Cenke Xu,[2] Zi Yang Meng,[3] and Zhong-Yi Lu[1]
[1]*Department of Physics, Renmin University of China, Beijing 100872, China*
[2]*Department of Physics, University of California, Santa Barbara, California 93106, USA*
[3]*Beijing National Laboratory for Condensed Matter Physics and Institute of Physics, Chinese Academy of Sciences, Beijing 100190, China*
(Received 7 April 2016; published 20 December 2016)

We study a lattice model of interacting Dirac fermions in $(2+1)$ dimensions space-time with an SU(4) symmetry. While increasing the interaction strength, this model undergoes a *continuous* quantum phase transition from a weakly interacting Dirac semimetal to a fully gapped and nondegenerate phase without condensing any Dirac fermion bilinear mass operator. This unusual mechanism for mass generation is consistent with recent studies of interacting topological insulators/superconductors, and also consistent with recent progress in the lattice QCD community.

DOI: 10.1103/PhysRevB.94.241111

Introduction. In the standard model of particle physics, all the matter fields, quarks and leptons, acquire their mass from "spontaneous symmetry breaking", or, equivalently, the condensation of the Higgs field [1–3]. The Higgs field couples to the bilinear mass operator of the Dirac fermion matter fields (except for the neutrinos), and hence the matters acquire a mass in the condensate. In the context of correlated electron systems, mass generation (or gap opening) due to interactions is also often a consequence of spontaneous symmetry breaking and the development of a certain long-range order. For example, in a superconductor the Cooper pairs condense, which spontaneously breaks the $U(1)$ charge symmetry of the electrons, and as a result the electrons acquire a mass gap at the Fermi surface. So, consensus has it that, in strongly interacting fermionic systems (either in condensed matter or high-energy physics), mass (or gap) generation is usually related to spontaneous symmetry breaking and the condensation of a fermion bilinear operator [4].

However, in condensed matter systems there exists an alternative mechanism for mass generation, which does not involve any spontaneous symmetry breaking or long-range order. The most well-known example is the fractional quantum Hall state, where a partially filled Landau level, which would be gapless without an interaction, is driven into a fully gapped state by a strong interaction. This gapped state has an unusual topological order and topological ground state degeneracy [5,6]. Recently, it was discovered that the phenomenon of "mass generation without symmetry breaking" can happen even without topological order. This mechanism was discovered in the context of interacting topological insulators, and it was found that some topological insulators/superconductors can be trivialized by interactions. Or, in other words, their boundary states, which without interactions are gapless Dirac fermions or Majorana fermions at one lower dimension, can be completely gapped out by interactions without topological degeneracy or condensing any fermion bilinear mass operators [7–19].

This new mechanism of mass generation was tested and confirmed numerically by both condensed matter [20] and lattice QCD [21–23] physicists, using quantum Monte Carlo simulation methods. These works provide evidence that the massless Dirac fermion phase and the massive quantum phase without any fermion mass condensation are connected by a single continuous quantum phase transition.

In this Rapid Communication, we construct a microscopic model in $(2+1)$ dimensions (D) with four flavors of complex fermions, by employing large-scale quantum Monte Carlo (QMC) simulations in an unbiased manner. We find that there indeed exists a single interaction-driven Dirac semimetal (DSM) to featureless Mott insulator (FMI) phase transition, which is continuous and does not involve any spontaneous symmetry breaking. We also provide an analysis of scaling behavior at this quantum critical point.

Model and method. We construct a model Hamiltonian with four flavors of fermions on a 2D honeycomb lattice at half filling with SU(4) symmetry:

$$\begin{aligned} \hat{H} &= H_{\text{band}} + H_{\text{int}}, \\ \hat{H}_{\text{band}} &= -t \sum_{\langle l,r\rangle\alpha} (-1)^{\alpha} (c^{\dagger}_{l\alpha} c_{r\alpha} + c^{\dagger}_{r\alpha} c_{l\alpha}), \\ \hat{H}_{\text{int}} &= V \sum_{r} (c^{\dagger}_{r1} c_{r2} c^{\dagger}_{r3} c_{r4} + c^{\dagger}_{r4} c_{r3} c^{\dagger}_{r2} c_{r1}), \end{aligned} \tag{1}$$

where $\alpha = 1,2,3,4$ in $\hat{H}_{\text{band}}$ stands for fermion flavors and $\langle l,r\rangle$ denotes the nearest-neighbor sites.

t is set as the energy unit throughout this Rapid Communication. The lattice geometry and Brillouin zone are shown in Figs. 1(a) and 1(b), respectively. This Hamiltonian has an SU(4) symmetry and is invariant under the transformation $\xi_r \to U\xi_r$ for any $U \in \text{SU}(4)$, with $\xi_r = (c^{\dagger}_{r1}, c_{r2}, c^{\dagger}_{r3}, c_{r4})^{\text{T}}$. The $(-1)^{\alpha}$ factor in the hopping term $\hat{H}_{\text{band}}$ is enforced by the SU(4) symmetry.

It is straightforward to check that, if we keep the system at half filling, then analogous to the usual case in graphene, all the lattice symmetries, such as 60° rotation, reflection, translation, time reversal, etc., together with the SU(4) flavor symmetry and particle-hole symmetry $c_{r\alpha} \to (-1)^{r} c^{\dagger}_{r\alpha}$, prohibit the gap opening of the Dirac fermions in the noninteracting limit, namely, any fermion bilinear mass operator of the Dirac fermion will break at least one of the symmetries.

To explore the ground state properties of the model in Eq. (1) in the presence of interactions, we employ the projector determinant quantum Monte Carlo (DQMC) method [24,25]; details of this calculation are presented in Sec. I of the

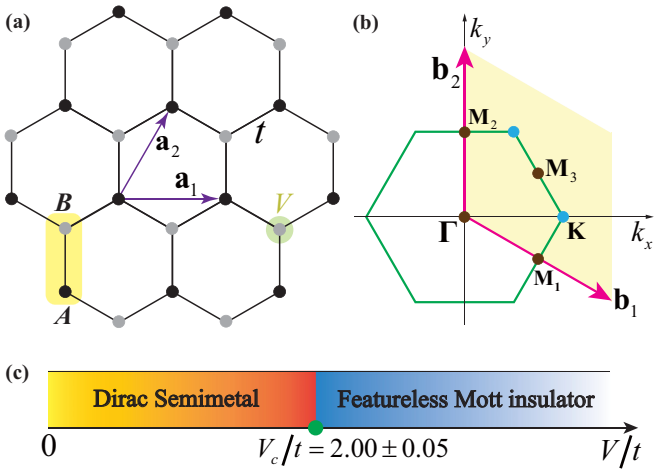

FIG. 1. Lattice geometry and phase diagram for the SU(4) symmetric model in Eq. (1). (a) The honeycomb lattice, whose unit cell is denoted by the yellow shaded rectangle. (b) The Brillouin zone. (c) Phase diagram for the model Eq. (1) obtained from QMC simulations. Two quantum phases, Dirac semimetal and featureless Mott insulator, are observed, which are connected by a continuous quantum phase transition located at $V_c/t = 2.00 \pm 0.05$.

Supplemental Material [26]. As discussed there, QMC is immune from the minus-sign problem for both the $V > 0$ and $V < 0$ cases. Comparisons between exact diagonalization and QMC simulations on a 2×2 system (eight lattice sites) are carried out as a sanity check. Numerical verification of the SU(4) symmetry of the model is also performed and presented in Sec. IV of the Supplemental Material [26]. In this Rapid Communication, we focus on the $V > 0$ case and the system sizes simulated are $L = 3$, 6, 9, 12, 15, and 18. We denote $N_s = 2L^2$ as the total number of lattice sites and $N = L^2$ as the number of unit cells.

Ground state phase diagram. The phase diagram of the SU(4) symmetric model in Eq. (1) is presented in Fig. 1(c). Two quantum phases, a gapless Dirac semimetal and a featureless Mott insulator, are observed, respectively. Furthermore, they are connected by a continuous quantum phase transition located at $V_c/t = 2.00 \pm 0.05$. While increasing the interaction strength V/t, we observe no spontaneous symmetry breaking. The FMI is gapped in both fermionic and bosonic channels (shown later) without any symmetry breaking.

The FMI is easy to understand from the $V \to +\infty$ limit. Since the interaction is on site, it is easy to perceive that, when $V \to +\infty$, the ground state is

$$|\Psi_g\rangle = \prod_r |\Psi_r\rangle = \prod_r \frac{1}{\sqrt{2}} \left(\prod_{\alpha=1}^{4} \xi_{r,\alpha}^\dagger - 1 \right) |0\rangle_\xi, \qquad (2)$$

where $|0\rangle_\xi$ is the vacuum of ξ fermions, and $\hat{H}_{\rm int}|\Psi_g\rangle = -VN_s|\Psi_g\rangle$ (this state is at half filling, written with the $c_{r,\alpha}$ fermions). $|\Psi_g\rangle$ is a direct product state of SU(4) singlets [18,27–29]. Since obviously $|\Psi_g\rangle$ preserves all the symmetries (including flavor, lattice, and time-reversal and particle-hole symmetries) of the system, any Dirac fermion mass operator should have a zero expectation value in this state. Hence, the wave function $|\Psi_g\rangle$ describes a symmetric featureless Mott insulator. Note our state has a different flavor symmetry and number of states per site compared with another featureless Mott insulator proposed recently [30].

It is well known that the (2+1)D massless Dirac fermions are stable against weak short-range interactions [25]. The transition from the weakly interacting DSM to the strongly coupled FMI as a function of V/t is the main issue that we explore here. As it will become clear in the following, a direct continuous quantum phase transition from DSM to FMI is revealed by our QMC simulations. More importantly, there is no spontaneous symmetry breaking and no fermion bilinear condensation across this transition.

$O(6)$ order vectors and excitation gaps. To verify our conclusion, we need to analyze the behavior of all the Dirac fermion mass operators. Because there is only an on-site interaction in our model, we will focus on Dirac mass operators that are defined on site, which is most likely favored by the interaction at the mean field level. We begin with order parameters that transform as a vector under SU(4) symmetry. Such order parameters can be combined into two sets of SO(6) $\sim$ SU(4) vector $\boldsymbol{\phi}$ and pseudovector $\boldsymbol{\psi}$ [26],

$$\begin{aligned}
\phi_{r1} + i\psi_{r1} &= (c_{r1}^\dagger c_{r4} + c_{r3}^\dagger c_{r2}),\\
\phi_{r2} + i\psi_{r2} &= (c_{r1}^\dagger c_{r3}^\dagger + c_{r2} c_{r4}),\\
\phi_{r3} + i\psi_{r3} &= (c_{r1}^\dagger c_{r2} - c_{r3}^\dagger c_{r4}),\\
\phi_{r4} + i\psi_{r4} &= i(c_{r1}^\dagger c_{r4} - c_{r3}^\dagger c_{r2}),\\
\phi_{r5} + i\psi_{r5} &= i(c_{r1}^\dagger c_{r3}^\dagger - c_{r2} c_{r4}),\\
\phi_{r6} + i\psi_{r6} &= i(c_{r1}^\dagger c_{r2} + c_{r3}^\dagger c_{r4}),
\end{aligned} \qquad (3)$$

and the SO(6) symmetry rotates the six components to one another, respectively. The fact that $\boldsymbol{\phi}$ and $\boldsymbol{\psi}$ are mass operators of the Dirac fermions is more explicit in the basis of ξ_r fermions. In the long-wavelength limit, we can express ξ_r in terms of the low-energy modes ξ_K ($\xi_{K'}$) around the K (K') point in the Brillouin zone, as $\xi_{\mathbf{r}} \sim \xi_K e^{i\mathbf{K}\cdot\mathbf{r}} + \xi_{K'} e^{-i\mathbf{K}\cdot\mathbf{r}}$. The low-energy effective band Hamiltonian reads

$$\begin{aligned}
H_{\rm band} \simeq \int d^2\mathbf{x}\, &\xi_K^\dagger v_F(+i\partial_x\sigma^x + i\partial_y\sigma^y)\xi_K\\
&+ \xi_{K'}^\dagger v_F(-i\partial_x\sigma^x + i\partial_y\sigma^y)\xi_{K'}.
\end{aligned} \qquad (4)$$

The operators $\boldsymbol{\phi} + i\boldsymbol{\psi}$ are SU(4) flavor-mixing pairings of the ξ_r fermions, which take the form of $M_{\alpha\beta}\xi_{K,\alpha}\xi_{K',\beta}$ ($\alpha,\beta = 1,2,3,4$ label the flavors), with M being a (full rank) 4×4 antisymmetric matrix. The six orthogonal bases of the 4×4 antisymmetric matrices correspond to the six components in $\boldsymbol{\phi} + i\boldsymbol{\psi}$. It is easy to see that $\boldsymbol{\phi} + i\boldsymbol{\psi}$ can gap out the Dirac fermions, which are potentially favored to order at the mean field level.

Due to the SU(4) symmetry, the correlation functions $\langle\phi_{r,\alpha}\phi_{r',\alpha}\rangle$ must be identical for all α. The same condition holds for $\boldsymbol{\psi}$. This is numerically checked and shown in Sec. IV of the Supplemental Material [26].

To determine whether the system develops long-range orders in $\boldsymbol{\phi}$ and $\boldsymbol{\psi}$ with increasing V/t, we measure their

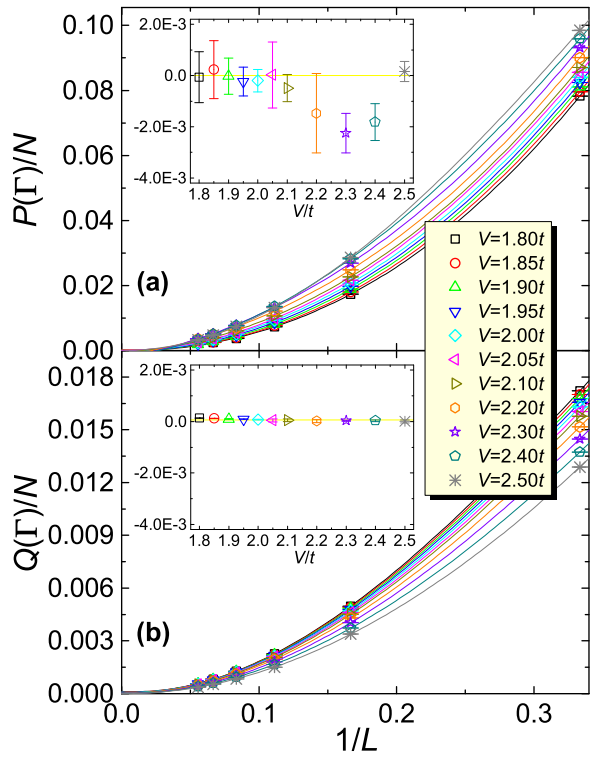

FIG. 2. Extrapolation of structure factors (a) $P(\mathbf{\Gamma})/N$ and (b) $Q(\mathbf{\Gamma})/N$ over the inverse system size $1/L$ by cubic polynomials. The insets show the extrapolated values at the thermodynamic limit. From the results, both of the $O(6)$ orders are absent across the DSM-FMI phase transition.

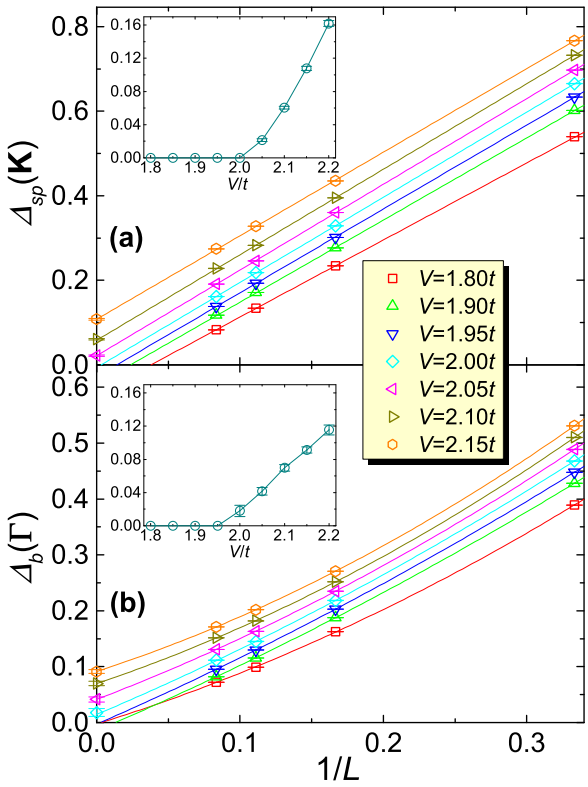

FIG. 3. Extrapolation of (a) single-particle (fermionic) gap $\Delta_{\rm sp}(\mathbf{K})$ and (b) $O(6)$ order correlation (bosonic) gap $\Delta_b(\mathbf{\Gamma})$ over the inverse system size $1/L$ by linear and quadratic polynomials, respectively. The insets show the extrapolated gap values at the thermodynamic limit. Both excitation gaps open at $V_c/t = 2.00 \pm 0.05$.

structure factors as follows,

$$P(\mathbf{k}) = \frac{1}{12N}\sum_{\gamma=A,B}\sum_{\eta=1}^{6}\sum_{ij} e^{i\mathbf{k}\cdot(\mathbf{R}_i-\mathbf{R}_j)}\langle\phi_{i\gamma,\eta}\phi_{j\gamma,\eta}\rangle,$$
$$Q(\mathbf{k}) = \frac{1}{12N}\sum_{\gamma=A,B}\sum_{\eta=1}^{6}\sum_{ij} e^{i\mathbf{k}\cdot(\mathbf{R}_i-\mathbf{R}_j)}\langle\psi_{i\gamma,\eta}\psi_{j\gamma,\eta}\rangle, \quad (5)$$

where i,j label unit cells. Through the extrapolation of $P(\mathbf{\Gamma})/N$ and $Q(\mathbf{\Gamma})/N$ over the inverse system size $1/L$, we can obtain the value of $\langle\boldsymbol{\phi}\rangle$ and $\langle\boldsymbol{\psi}\rangle$ in the thermodynamic limit. The results for $V/t = 1.8$–2.5 across the phase transition are shown in Figs. 2(a) and 2(b), and the insets are the extrapolated values. We notice that the $Q(\mathbf{\Gamma})/N$ is one order of magnitude smaller than $P(\mathbf{\Gamma})/N$. Combining the results of $P(\mathbf{\Gamma})/N$ and $Q(\mathbf{\Gamma})/N$, we conclude that neither $\boldsymbol{\phi}_l$ nor $\boldsymbol{\psi}_l$ develops long-range order.

As for the dynamic properties, the single-particle (fermion) gap can be extracted from the dynamic single-particle Green's function as

$$G(\mathbf{k},\tau) = \frac{1}{8N}\sum_{\gamma=A,B}\sum_{\alpha=1}^{4}\sum_{ij} e^{i\mathbf{k}\cdot(\mathbf{R}_i-\mathbf{R}_j)}[G(\tau)]^{\alpha}_{i\gamma,j\gamma}, \quad (6)$$

where $[G(\tau)]^{\alpha}_{i\gamma,j\gamma} = \langle T_\tau[c_{i\gamma,\alpha}(\tau)c^{\dagger}_{j\gamma,\alpha}(0)]\rangle$. The Green's function scales as $G(\mathbf{k},\tau) \propto e^{-\Delta_{\rm sp}(\mathbf{k})\tau}$ under the limit $\tau\to\infty$ and $\Delta_{\rm sp}(\mathbf{k})$ is the single-particle gap. Similarly, the bosonic gap $\Delta_b(\mathbf{\Gamma})$ can be extracted from the following dynamic correlation as

$$P(\mathbf{k},\tau) = \frac{1}{12N}\sum_{\gamma=A,B}\sum_{\eta=1}^{6}\sum_{ij} e^{i\mathbf{k}\cdot(\mathbf{R}_i-\mathbf{R}_j)}[P(\tau)]^{\eta}_{i\gamma,j\gamma}, \quad (7)$$

where $[P(\tau)]^{\eta}_{i\gamma,j\gamma} = \langle T_\tau[\phi_{i\gamma,\eta}(\tau)\phi_{j\gamma,\eta}(0)]\rangle$. Note that the bosonic gaps extracted from the $\boldsymbol{\phi}_l$ correlation and $\boldsymbol{\psi}_l$ correlation should be equal, which has also been numerically confirmed (see the Supplemental Material, Sec. IV [26]). Both results of the single-particle gap and the bosonic gap are shown in Fig. 3. Through the extrapolation of the gap, we observe that the single-particle gap opens at $V/t = 2.0$–2.05, while the bosonic gap opens at $V/t = 1.95$–2.0. This tiny difference between the critical points extracted from the fermionic and bosonic gap is attributed to the finite-size effect, and the possibility of an intermediate phase with either $\boldsymbol{\phi}_r$ or $\boldsymbol{\psi}_r$ long-range order can be ruled out, as otherwise the single-particle gap should open before the bosonic gap while increasing V. Combining all data above, we conclude that the DSM-FMI phase transition occurs at $V_c/t = 2.00 \pm 0.05$.

Other possible long-range orders. In addition to the two sets of $O(6)$ order parameters, there are other Dirac fermion mass operators (or order parameters) which may develop long-range order due to the interaction in Eq. (1). All the possible

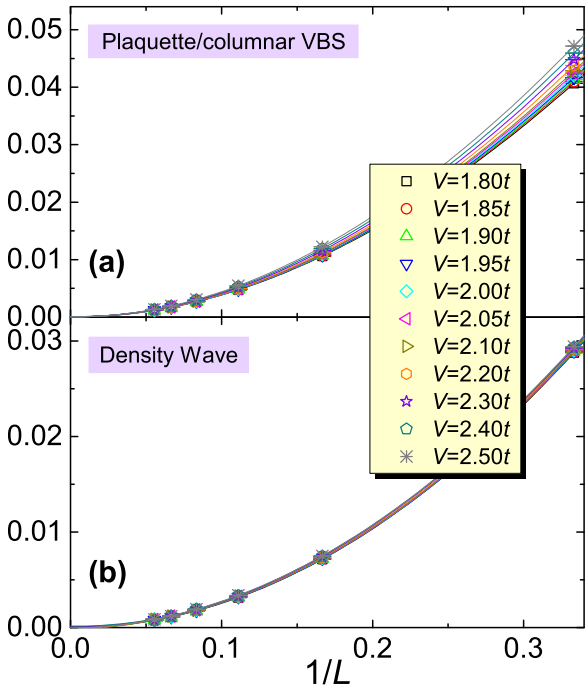

FIG. 4. Extrapolation of structure factors divided by N for (a) plaquette/columnar VBS order, and (b) density wave order, over inverse system size $1/L$ by cubic polynomials, across the DSM-FMI phase transition. The results show that neither of these two long-range orders exist near the DSM-FMI phase transition.

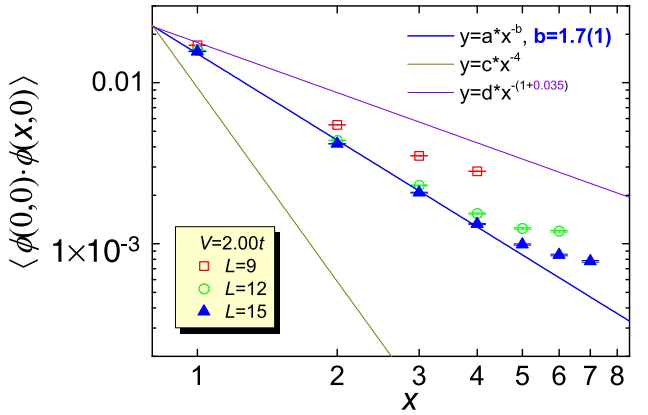

FIG. 5. Blue line: Fit of the spatial correlation of $O(6)$ order parameter $\boldsymbol{\phi}$ along the $\mathbf{a}_1$ direction for $L = 12,15$ systems as $\langle\phi(0,0)\cdot\phi(x,0)\rangle$ at $V = V_c$. The obtained anomalous dimension $\eta = 0.7\pm0.1$. Dark green line: $\frac{1}{x^4}$, the behavior of $O(6)$ correlation at $V = 0$. Violet line: $\frac{1}{x^{1.035}}$, the behavior of $O(6)$ correlation at the $(2+1)$D Wilson-Fisher $O(6)$ transition.

Dirac mass operators are summarized in the Supplemental Material, Sec. III [26]. The results of four representative order parameters, including the plaquette/columnar valence bond solid (VBS) order, quantum Hall-like insulating phase (loop current order), next-nearest-neighbor (NNN) pairing order, and the density wave order, are numerically measured and two of them (the plaquette/columnar VBS and density wave order) are presented in Fig. 4 (the two other are presented in the Supplemental Material, Sec. III [26]). From the extrapolations of structure factors, we conclude that none of these operators develops long-range order near the DSM-FMI phase transition.

Continuous DSM-FMI phase transition. The data of excitation gaps and all possible order parameters reveal the unusual mechanism of fermion mass generation without condensing any fermion bilinear mass operator. To further explore the nature of the DSM-FMI transition, we have also measured the first derivative of the ground state energy $\langle\rho\rangle = \frac{1}{N_s}\frac{\partial\langle\hat{H}\rangle}{\partial V} = \frac{1}{N_s}\sum_r (c^\dagger_{r1}c_{r2}c^\dagger_{r3}c_{r4} + c^\dagger_{r4}c_{r3}c^\dagger_{r2}c_{r1})$. The results are presented in Fig. S6 in the Supplemental Material [26]. The converged $\langle\rho\rangle$ with $L = 15$ and $L = 18$ changes continuously across the DSM-FMI phase transition, indicating a continuous phase transition. Besides, we have also measured the spatial correlation functions of the $O(6)$ order parameter $\boldsymbol{\phi}$ along the $\mathbf{a}_1$ direction for $L = 9$, 12, and 15 at $V = V_c$, and the results are shown in Fig. 5. In the log-log plot, the convergence of the slope for $L = 12$ and $L = 15$ can be seen. At the quantum critical point, $\langle\phi(0,0)\cdot\phi(x,0)\rangle$ decays at sufficiently long distances as $1/x^{1+\eta}$, where η is the anomalous dimension. The fit of the data gives $\eta = 0.7 \pm 0.1$. Such an anomalous dimension is much larger than that of the Wilson-Fisher fixed point of the $(2+1)$D $O(6)$ transition with $\eta = 0.035$ obtained from ϵ expansion [31]. Also, the spatial correlation of the $O(6)$ order parameter of the noninteracting Dirac fermions is shown in Fig. 5, which has a form of $1/x^4$.

Conclusions. We find a continuous DSM-FMI transition without any spontaneous symmetry breaking in a simple model of four-flavor fermions with SU(4) symmetry. The quantum critical point at $V_c/t = 2.00 \pm 0.05$ separates the gapless Dirac semimetal from the featureless Mott insulator. Such a mechanism of mass generation without fermion bilinear condensation is consistent with previous studies from the lattice QCD community [21–23]. More interestingly, in our investigations, the excitation gaps and an exhaustive exclusion of symmetry breaking are directly accessed and a large anomalous dimension η at the DSM-FMI transition is revealed. The entanglement properties in our model, especially close to the quantum critical point, should also be very interesting and recently have become available to measure in the DQMC framework [32–34]. It is certain worthwhile to investigate such properties in a future study.

Acknowledgments. We would like to thank S. Chandrasekharan, S. Catterall, H.-T. Ding, and F. F. Assaad for helpful discussions. The numerical calculations were carried out at the Physical Laboratory of High Performance Computing in RUC, the Center for Quantum Simulation Sciences in the Institute of Physics, Chinese Academy of Sciences, as well as the National Supercomputer Center in Tianjin (TianHe-1A) and GuangZhou (TianHe-2). Z.Y.M. is supported by the Ministry of Science and Technology (MOST) of China under Grant No. 2016YFA0300502 and the National Thousand-Young-Talents Program of China. H.-Q.W., Y.-Y.H., Z.Y.M., and Z.-Y.L. acknowledge support from the National Natural Science Foundation of China (Grants No. 91421304, No. 11474356, No. 11421092, and No. 11574359). Y.-Z.Y. and C.X. are supported by the David and Lucile Packard Foundation and NSF Grant No. DMR-1151208.

[1] P. W. Higgs, Phys. Rev. Lett. **13**, 508 (1964).
[2] F. Englert and R. Brout, Phys. Rev. Lett. **13**, 321 (1964).
[3] G. S. Guralnik, C. R. Hagen, and T. W. B. Kibble, Phys. Rev. Lett. **13**, 585 (1964).
[4] V. L. Ginzburg and L. D. Landau, Zh. Eksp. Teor. Fiz. **20**, 1064 (1950).
[5] X.-G. Wen, Int. J. Mod. Phys. B **4**, 239 (1990).
[6] X.-G. Wen and Q. Niu, Phys. Rev. B **41**, 9377 (1990).
[7] L. Fidkowski and A. Kitaev, Phys. Rev. B **81**, 134509 (2010).
[8] L. Fidkowski and A. Kitaev, Phys. Rev. B **83**, 075103 (2011).
[9] X.-L. Qi, New J. Phys. **15**, 065002 (2013).
[10] H. Yao and S. Ryu, Phys. Rev. B **88**, 064507 (2013).
[11] S. Ryu and S.-C. Zhang, Phys. Rev. B **85**, 245132 (2012).
[12] Z.-C. Gu and M. Levin, Phys. Rev. B **89**, 201113 (2014).
[13] L. Fidkowski, X. Chen, and A. Vishwanath, Phys. Rev. X **3**, 041016 (2013).
[14] C. Wang and T. Senthil, Phys. Rev. B **89**, 195124 (2014).
[15] Y.-Z. You, Y. BenTov, and C. Xu, arXiv:1402.4151.
[16] Y.-Z. You and C. Xu, Phys. Rev. B **90**, 245120 (2014).
[17] T. Morimoto, A. Furusaki, and C. Mudry, Phys. Rev. B **92**, 125104 (2015).
[18] Y.-Y. He, H.-Q. Wu, Y.-Z. You, C. Xu, Z. Y. Meng, and Z.-Y. Lu, Phys. Rev. B **93**, 115150 (2016).
[19] R. Queiroz, E. Khalaf, and A. Stern, Phys. Rev. Lett. **117**, 206405 (2016).
[20] K. Slagle, Y.-Z. You, and C. Xu, Phys. Rev. B **91**, 115121 (2015).
[21] V. Ayyar and S. Chandrasekharan, Phys. Rev. D **91**, 065035 (2015).
[22] S. Catterall, J. High Energy Phys. 01 (2016) 121.
[23] V. Ayyar and S. Chandrasekharan, Phys. Rev. D **93**, 081701 (2016).
[24] F. Assaad and H. Evertz, in *Computational Many-Particle Physics*, edited by H. Fehske, R. Schneider, and A. Weiße, Lecture Notes in Physics Vol. 739 (Springer, Berlin, 2008), pp. 277–356.
[25] Z. Y. Meng, T. C. Lang, S. Wessel, F. F. Assaad, and A. Muramatsu, Nature (London) **464**, 847 (2010).
[26] See Supplemental Material at http://link.aps.org/supplemental/10.1103/PhysRevB.94.241111 for discussions on the implementation of QMC, absence of the minus-sign problem, analysis of the ground state, possible symmetry breaking orders, etc.
[27] Y.-Y. He, H.-Q. Wu, Z. Y. Meng, and Z.-Y. Lu, Phys. Rev. B **93**, 195163 (2016).
[28] Y.-Y. He, H.-Q. Wu, Z. Y. Meng, and Z.-Y. Lu, Phys. Rev. B **93**, 195164 (2016).
[29] Y.-Z. You, Z. Bi, D. Mao, and C. Xu, Phys. Rev. B **93**, 125101 (2016).
[30] C.-C. Chen, L. Muechler, R. Car, T. Neupert, and J. Maciejko, Phys. Rev. Lett. **117**, 096405 (2016).
[31] J. Zinn-Justin, *Quantum Field Theory and Critical Phenomena* (Clarendon, Oxford, UK, 2002).
[32] T. Grover, Phys. Rev. Lett. **111**, 130402 (2013).
[33] F. F. Assaad, T. C. Lang, and F. Parisen Toldin, Phys. Rev. B **89**, 125121 (2014).
[34] F. F. Assaad, Phys. Rev. B **91**, 125146 (2015).